Journal of Solid Mechanics Vol. 11, No. 2 (2019) pp. 323-340
DOI: 10.22034/JSM.2019.665256

Coupled Axial-Radial Vibration of Single-Walled Carbon Nanotubes Via Doublet Mechanics

Z. Azimzadeh, A. Fatahi-Vajari*

Young Researchers and Elite Club, Yadegar-e-Imam Khomeini (RAH) Shahr-e-Rey Branch, Islamic Azad University, Tehran, Iran

Received 18 February 2019; accepted 10 April 2019

ABSTRACT

This paper investigates the coupled axial-radial (CAR) vibration of single-walled carbon nanotubes (SWCNTs) based on doublet mechanics (DM) with a scale parameter. Two coupled forth order partial differential equations that govern the CAR vibration of SWCNTs are derived. It is the first time that DM is used to model the CAR vibration of SWCNTs. To obtain the natural frequency and dynamic response of the CAR vibration, the equations of motion are solved and the relation between natural frequencies and scale parameter is derived. It is found that there are two frequencies in the frequency spectrum and these CAR vibrational frequencies are complicated due to coupling between two vibration modes. The advantage of these analytical formulas is that they are explicitly dependent to scale parameter and chirality effect. The influence of changing some geometrical and mechanical parameters of SWCNT on its CAR frequencies has been investigated, too. It is shown that the chirality and scale parameter play significant role in the CAR vibration response of SWCNTs. The scale parameter decreases the higher band CAR frequency compared to the predictions of the classical continuum models. However, with increase in tube radius and length, the effect of the scale parameter on the natural frequencies decreases. The lower band CAR frequency is nearly independent to scale effect and tube diameter. The CAR frequencies of SWCNTs decrease as the length of the tube increases. This decreasing is higher for higher band CAR frequency. To show the accuracy and ability of this method, the results obtained herein are compared with the existing theoretical and experimental results and good agreement is observed.

Keywords : Coupled axial-radial vibration; Doublet mechanics; Natural frequency; Scale parameter; Single-walled carbon nanotubes.

1 INTRODUCTION

AT nanoscale levels, the mechanical characteristics of nanostructures are often significantly different from their behavior at macroscopic scale due to the inherent size effects. Such characteristics greatly affect the

*Corresponding author. Tel.: +98 2165649901.
E-mail address: alirezafatahi@shriau.ac.ir (A. Fatahi-Vajari).

performance of nanoscale materials or structures and nanoinstruments. Theory of classical continuum mechanics (CCM) is used to develop the equations of motion whereas the small scale effects due to atomic scale of the lattice structures of carbon nanotubes (CNTs) are not taken into account. Moreover, the length scales associated with nanotubes are often sufficiently small to call the applicability of classical continuum models into question [1]. Banks et al. provided a review of equations of motion in a continuum and completed the set of equations with presenting and discussing a number of specific forms for the constitutive relationships between stress and strain proposed in the literature for both elastic and viscoelastic materials [2]. Classical continuum mechanics modelling assumptions are conducive to erroneous results, when applied to material domains where the typical microstructural dimension is comparable with the structural ones [3].

Currently, various elegant modifications to continuum mechanics have been proposed to incorporate scale and microstructural features into the theory. Problems studied by means of a variety of approaches are just different aspects of the same general problem. The most used methods for today's research in applied mechanics for new materials like nano can be categorized in generalized continuum mechanics theories [4-8] and atomistic-discrete models [9-12]. The nonlocal and higher gradients continuum mechanics was conceived already in Piola's works and Many nonlocal continuum theories were formulated since the first formulation by Piola [7]. In nonlocal theories, as opposed to local theories, it is assumed that particles further apart will influence each other. Several nonlocal theories exist which consider the long-range interactions between materials particles. These theories can be broadly divided into two major groups [13]:

1. Weakly nonlocal theories such as strain gradient theories and modified couple stress theories, where stress at each point depends not only on the strain but also on the derivatives of the strain. These are non CCM theories in the sense that they account couple stress effect and the material length scale comes in through a constitutive equation relating the couple stress tensor and curvature tensor. Strain-gradient theory introduced by Mindlin [6] may be used to accurately model the response of solids and structures in small scales. There are three separate forms in the theory called generally Form I, Form II and Form III. The convergence of the strain-gradient and CCM methods deemed for a moderately large deformation and it showed that the theories have the same results by growing the size of the body when dimensions are relatively bigger than the length scale. Unlike CCM, the strain energy density function for strain gradient theory includes additional terms due to the couple stress. The strain energy potential in CCM theories only depends on the strains, whereas in the strain gradient theory it depends not only on the strain but also on the gradients of the strain. This introduces a material length scale (a size-dependent property) into the formulation. Polizzotto compared the stress gradient model with strain gradient model featured by a constitutive equation and concluded that the main differences are pointed out in relation to their mechanical behaviors and in particular to the relevant surface effects, as well as to the computational aspects [8]. Khodabakhshi and Reddy showed that both the strain gradient theory and the von Karman nonlinearity have a stiffening effect, and therefore, reduce the displacements. The influence is more prominent in thick beams. In order to take account of the geometric nonlinearity, Beheshti studied finite deformation in the strain gradient continuum based on the infinitesimal strain tensor given the Green–Lagrange strain tensor [14].

2. Strongly nonlocal theories such as Eringen integral theory and peridynamic theory, where stress at each point depends on the strain at all points within a domain through an integral. Several papers have been published in the last decade in these two areas deal with beams, plates, and shells. A good list of references on these two classes of models can be found in [15-19]. Kiani [15] developed the lateral buckling of two- and three dimensional (2D and 3D) ensembles of vertically aligned SWCNTs based on the nonlocal stress theory. Based on both discrete and continuous models, the critical axial buckling loads for both 2D and 3D ensembles of SWCNTs are obtained. Fatahi-Vajari and Azimzadeh studied nonlinear axial vibration of SWNTs using Homotopy perturbation method [16]. Using nonlocal higher order beam theory, traveling transverse waves in vertically aligned jungles of SWCNTs in the presence of a longitudinal magnetic field are studied by Kiani [17] using both nonlocal discrete and continuous models. Aydogdu investigated axial vibration analysis of nanorods embedded in an elastic medium using nonlocal elasticity [18]. Kiani developed new nonlocal discrete and continuous models to obtain fundamental frequencies in free bending vibration of 2D ensembles of SWCNTs leads to the definition of in-plane and out-of-plane flexural behaviors for such nanostructures [19].

The common feature of all nonlocal theories is the introduction of material length scales which represent certain microstructural features (e.g., lattice structure). Most nonlocal theories exhibit a stiffening effect. This effect is more significant when certain dimension of a structure like thickness in the case of beams, plates, and shells, becomes comparable to the scale parameter. The Eringen method consists in both the differential constitutive equations and integral type. This means that the nonlocality effects of the original integral-type problem enter into the differential-type problem as gradient effects originating from a source identified with the Cauchy stress σ. In other words, the original nonlocal integral-type model is replaced with a stress gradient model. Indeed, the latter model finds itself in

strong contrast with the well-known strain gradient model widely employed to describe size effects and other phenomena of small scale solids [13].

Various methods for simulating materials at an atomic level are existent, including lattice dynamics (LD), molecular dynamics (MD) and quantum mechanical (QM) methods [10]. LD studies vibrations of the atomic nuclei of solid crystals, the nuclei being considered as material points (particles) mutually bonded by elastic interatomic forces [20]. LD is based on the following far-reaching assumptions. Firstly, any crystal is an infinite lattice structure. Secondly, the crystal obeys some devised periodic boundary conditions (PBC). Therefore, in general, LD is incompatible with arbitrary boundary conditions [20]. The other atomistic method is MD. Applying MD, every single atom or molecule in CNTs is seen as a discrete mass point and the bonding forces between each pair of neighboring atoms obey Newton's laws of motion [5]. MD model usually employs simplifications, such as regularity of particle distribution, symmetry and periodicity. In practical engineering applications, for problems of micron size and up, this model is not of practical use because it requires enormous computational effort which cannot be handled with today's computer technology [21]. MD simulations are restricted to small scale systems and to short time intervals [18]. Another atomistic method is QM which avoids a direct analysis of the nanostructure considered made by a set of atoms. Indeed, the structure of the nanostructure can be reduced to the analysis of an atomic lattice of N particles. This system, using CCM, would be associated with the matrix form of the equation of motion [11]. A solution of the QM equation including all relevant interactions in solids is computationally highly overbearing and is available with only high-speed computers. Even with increasing computational resources, a series of approximations must be employed in order to render a comprehensive solution for any non-trivial system feasible and it is nowadays not only possible to simulate certain experimental conditions and set-ups at an unprecedented level of accuracy without any experimental input, but also to design new materials with tailored properties before actually casting them [12]. Full QM treatments remain all but intractable at present for more than a few hundred atoms [9]. Another challenge in developing QM methods is that it uses translational symmetry and dealing with equations for which there is no solution [10].

One particular theory that has recently been applied to materials with microstructure is doublet mechanics (DM). This theory originally developed by Granik [22], has been applied to granular materials by Granik and Ferrari [4] and Ferrari et al. [20]. In DM micromechanical models, solids are represented as arrays of points, particles or nodes at finite distances. This theory has shown good promise in predicting observed behaviors that are not predictable using continuum mechanics. Such behaviors include the so-called Flamant paradox (Ferrari et al., [20]), where in a half-space under compressive boundary loading, continuum theory predicts a completely compressive stress field while observations indicate regions of tensile stress. Other anomalous types of behavior include dispersive wave propagation. Ferrari et al. reformulated DM using a finite element approach with the aim of further expanding the potential applications of this theory [23]. Some applications of DM in biomechanics and nanomechanics are given in [24- 25]. Fang et al. [26] studied plane wave propagation in a cubic tetrahedral assembly using DM. Additional applications of doublet mechanics are given in [27- 32].

It should be noted that The nonlocal theory is deductive, in the sense that it employs field variables of intrinsic macroscopic nature (i.e, the strain and stress tensors), without explicit connections with the underlying discrete material microstructure [3]. Also, the total number of elastic macroconstants in the nonlocal theory is relatively large [6]. It should be pointed out that the nonlocal theory is phenomenological in nature. That is, unlike DM the nonlocal theory is developed following a simplified pattern without considering a particular microstructure [20]. Under such an approach the parameters of the microstructure are not included in the mathematical model directly as in DM. The microstructural parameters enter the nonlocal theory indirectly because it is implicitly contained in the macrotensors of elasticity. In other words, unlike the elastic macrotensors in DM, the elastic macrotensors in the nonlocal theory are unknown functions of the underlying microstructural parameters [20]. Consequently, the total number of elastic macroconstants in the nonlocal theory is considerably larger than that in DM. So even in the simplest nonlocal theory (grade two) there are many elastic macroconstants to be obtained experimentally. Clearly, this is practically very difficult to accomplish, not to mention the additional macroconstants required in more complex theories of materials of grade three and higher [20]. Nonlocal theory is deductive, in the sense that it employs field variables of intrinsic macroscopic nature (i.e, the strain and stress tensors), without explicit connections with the underlying discrete material microstructure [3]. With this introduction in mind, DM hasn't limitations mentioned in other theories such as CCM, atomistic methods and nonlocal theories.

Single-walled carbon nanotubes (SWCNTs) are tiny cylinders made from carbon [33]. A SWCNT can be described as a single layer of a graphite crystal that is rolled up into a seamless circular cylinder, one atom thickness, usually with a small number of carbon atoms along the circumference and a long length along the cylinder axis [34]. SWCNTs have many unique, fascinating properties. They are very strong and have extremely light weight. They are excellent conductors of heat, and transport electrons easily. The properties of CNTs depend strongly on their

microscopic structure [33]. The investigation of SWCNTs on the nanoscale is very important, since they are commonly used as resonators and sensors whose dynamic behavior needs to be understood. To demonstrate their applicability, some production techniques for making SWCNTs are explained in the [35-37]. Zhang et al. determined the vibration frequencies of SWCNTs using extensive MD simulations and Timoshenko beam modeling are performed to for SWCNTs with various aspect ratios, boundary conditions, chiral angles and initial strain [38]. Kiani studied the transverse vibrations of 3D vertically aligned periodic arrays of SWCNTs in presence of both longitudinal magnetic and thermal fields using nonlocal higher-order beam theory [39]. Ghorbanpour Arani et al. investigated the axial and torsional wave propagation in a double-walled carbon nanotube (DWCNT) embedded on elastic foundations using nonlocal continuum shell theory [40]. Fatahi-vajari and Imam studied axial vibration of SWCNTs using DM and obtain the natural frequency which was explicitly dependent to scale parameter [41]. Basirjafari et al. obtained an exact formula for the radial breathing mode (RBM) frequencies of triple-walled carbon nanotubes (TWCNTs) using symbolic package in MAPLE software [42]. To take into account the van der Waals (vdW) forces between adjacent SWCNTs because of their bidirectional transverse displacements, Kiani developed a linear model using Hamilton's principle based on the nonlocal Rayleigh, Timoshenko, and higher-order beam theories [43]. Das et al. studied inextensional vibrations of Zigzag SWCNTs using nonlocal elasticity theories and molecular mechanics simulations employing MM3 potential [44]. Fatahi-Vajari and imam studied RBM vibration of SWCNTs using DM and obtain the natural frequency which was explicitly dependent to scale parameter [45]. Li et al. took into account coupling effects of lateral, torsional and axial vibrations and a lumped-parameter nonlinear dynamic model of helical gear rotor- bearing system to obtain the transmission system dynamic response to the changes of different parameters [46]. Kiani studied longitudinal and transverse waves propagation in SWCNTs induced by friction between the nanoparticle and the SWCNTs, mass weight of the nanoparticle, and the interactional vdW forces between the constitutive atoms of the nanoparticle and those of the SWCNT using nonlinear-nonlocal continuum theory of Eringen [47]. Gupta and Batra studied Axial, torsional and RBM vibrations of free–free unstressed SWCNTs of different helicities using the MM [48]. It should be pointed out that RBM frequency is usually the strongest feature in Raman spectra which plays a crucial role in the experimental determination of the geometrical properties of SWCNTs. RBM frequencies are very useful for identifying a given material containing SWCNTs, through the existence of RBM modes, and for characterizing the nanotube diameter distribution in the sample through inverse proportionality of the RBM frequency to the tube diameter [49].

The SWCNTs may be subjected to some heavy and complex dynamic loadings caused by different sources. By producing different states of stress, these loads might result in excess vibrations and may lead to failure. Two important forms of vibrations that have been identified for SWCNTs are axial and radial vibrations. It should be pointed out that flexural (bending) vibration of SWCNTs also called fundamental vibration is very important vibration in nanostructure. To this end, many researchers have been studied about this vibration mode but the other vibration mode (spatially the coupled vibration) has not been investigated more. On the other hand, it can be seen from the previous works on the vibration of SWCNTs that most of existing SWCNTs systems were usually regarded as one vibrational mode systems, and the others vibrational modes were ignored. The coupled vibration of SWCNTs is an interesting subject because of the complexity of the equations and the analytical solutions are difficult to obtain. The axial-radial coupling vibration of the SWCNTs can lead to severe vibration, and this energy boosts the amplitude of the vibration and may leads to the early fatigue of tools and the reduction of bit life. If not taken into consideration, the effect of coupled vibration can not only reduce the calculation accuracy, but also lose some important characteristics of the CNTs. Therefore, it is important to establish an accurate model for dynamic characteristics of the coupled vibrations of CNTs.

Considering the complexity of the practical dynamics of the SWCNT systems, the main purpose of this study is investigating and modeling a mechanism for the CAR vibration of the SWCNTs using a new theory called DM. CAR vibration analysis of nanotubes based on DM has not yet been investigated analytically and the present work attempts to consider such analysis. The governing differential equations for this case consist of two coupled partial differential equations with radial and longitudinal displacements as the variables. These two coupled equations are solved to obtain the natural frequencies which incorporate explicitly chirality and scale effects. This will reveal which key factors affect the CAR vibration and how they function, which can be a basis for the quantitative analysis of the coupling vibration of the SWCNTs. The fundamental frequencies of SWCNT in CAR vibration are validated with experimental, atomistic, and continuum modeling results reported in literature.

2 BRIEF REVIEW OF DM

Originally developed by Granik [10], DM is a micromechanical theory wherein solids are represented as arrays of points or nodes at finite distances. A pair of such nodes is referred to as a doublet and the nodal spacing distances introduce length scales into the microstructural theory. Each node in the array is allowed to have translation and rotation where small translational and rotational displacements are expanded in a convergent Taylor series about the nodal point. The order at which the series is truncated defines the degree of approximation employed. The lowest order case using only a single term in the series does not contain any length scales, while the terms beyond the first produce a multi-scale theory. In this way, kinematical microstrains of elongation, shear and torsion (about the doublet axis) are developed. Through appropriate constitutive assumptions, such microstrains can be related to the corresponding elongational, shear and torsional microstresses.

Applications of DM to geo-mechanical problems have been given by Granik and Ferrari [4] and Ferrari et al. [20]. For such applications, a granular interpretation of DM has been employed, in which the material is viewed as an assembly of circular or spherical particles.

A doublet being a basic constitutive unit in DM is shown in Fig. 1. Corresponding to the doublet (A,B), there exists a doublet or branch vector ζ_a connecting the adjacent particle centers and defining the doublet axis. The magnitude of this vector $\eta_a = |\zeta_a|$ called length scales simply the particle diameter for particles in contact. However, in general, the particles need not be in contact, and for this case the length scale η_a could be used to represent a more general microstructural feature.

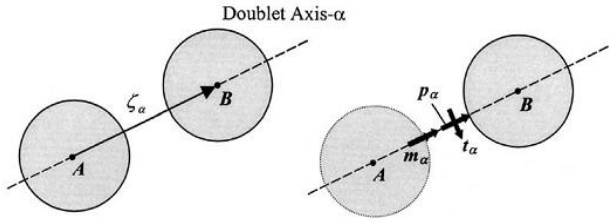

Fig.1
Doublet.

As mentioned above, the kinematics allow relative elongational, shearing and torsional motions between the particles, and this is used to develop an elongational microstress p_a, shear microstress t_a, and torsional microstress m_a as shown in Fig. 1. It should be pointed out that these microstresses are not second order tensors in the usual continuum mechanics sense. Rather, they are vector quantities that represent the elastic microforces and microcouples of interaction between doublet particles, examples of which include the interatomic forces between carbon molecules of a nanotube. The directions of microstresses depend on the doublet axes which are determined by the material microstructure. The microstresses are not continuously distributed but rather exist only at particular points in the medium being modeled by DM.

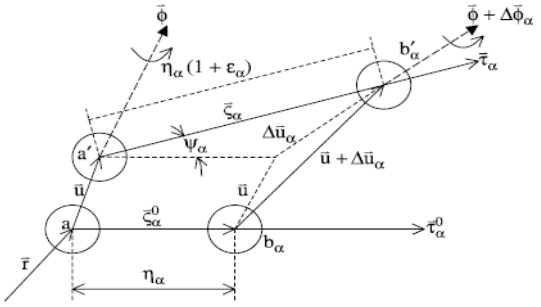

Fig.2
Translations of the doublet nodes a and b_a.

In Fig. 2, doublet (a,b_α) is shown to transform to doublet (a',b_α') as a result of kinematic translation. The superscript 0 for vectors indicates the initial configuration.

If $\boldsymbol{u}(\boldsymbol{x},t)$ is the displacement field representing the translation of node a, the incremental displacement may be written as:

$$\Delta \boldsymbol{u}_\alpha = u\left(\boldsymbol{x}+\boldsymbol{\zeta}_\alpha^0,t\right)-\boldsymbol{u}(\boldsymbol{x},t) \tag{1}$$

where $\boldsymbol{x}$ is the position vector of the particle.

Here, $\alpha=1,...,n$ while n is referred to the numbers of doublets. For the problem under study, it is assumed that the shear and torsional microdeformations and microstresses are negligible therefore only extensional microstrains and microstresses are assumed to exist.

It is further assumed that the relative displacement $\Delta \boldsymbol{u}_\alpha$ is small compared to the doublet separation distance $\eta_\alpha\left(\left|\Delta \boldsymbol{u}_\alpha\right| \ll \eta_\alpha\right)$ whereby it may be concluded that the unit vector $\boldsymbol{\tau}_\alpha = \boldsymbol{\tau}_\alpha^0$ [16].

The extensional microstrain scalar measure ϵ_α, representing the axial deformation of the doublet vector, is defined as [20]:

$$\epsilon_\alpha = \frac{\boldsymbol{\tau}_\alpha.\Delta \boldsymbol{u}_\alpha}{\eta_\alpha} \tag{2}$$

The incremental function in Eq. (2) is assumed to have a convergent Taylor series expansion written as [3]:

$$\epsilon_\alpha = \sum_{\chi=1}^{M} \frac{(\eta_\alpha)^{\chi-1}}{\chi!} \boldsymbol{\tau}_\alpha^0.\left(\boldsymbol{\tau}_\alpha^0.\nabla\right)^\chi \boldsymbol{u} \tag{3}$$

where ∇ is the gradient operator and η_α are the internal characteristic length scales. As mentioned above, the number of terms used in the series expansion of the local deformation field determines the order of the approximation in DM.

In DM, the relation between microstrain and microstress, neglecting torsional and shearing microstrain and temperature effects, is written as [21]:

$$p_\alpha = \sum_{\beta=1}^{n} A_{\alpha\beta}\epsilon_\beta \tag{4}$$

where p_α is the axial microstress along the doublet axes. An example of the axial microstress is the interatomic force between atoms or molecules located at the nodes of a general array such as a crystalline lattice. Eq. (4) can be interpreted as the constitutive equation in the linear theory of DM and $A_{\alpha\beta}$ is the matrix of the micromoduli of the doublet. The material is homogeneous if the matrix $A_{\alpha\beta}$ is constant throughout the body.

The unit vector $\boldsymbol{\tau}_\alpha^0$, known as the director vector, may be written as $\boldsymbol{\tau}_\alpha^0 = \tau_{\alpha j}^0 \boldsymbol{e}_j, j=1,2,3$ where $\tau_{\alpha j}^0, j=1,2,3$ are the cosines of the angles between the direction of the microstress vector and the coordinates and $\boldsymbol{e}_i, i=1,2,3$ are the unit vectors of the coordinate system.

In an isotropic medium capable of undergoing only local interactions, Eq. (4) is simplified as [1]:

$$p_\alpha = A_0\epsilon_\alpha \tag{5}$$

The relation between macrostresses and microstresses is written as [28]:

$$\sigma_{ij}^{(M)} = \sum_{\alpha=1}^{n} \tau_{\alpha i}^0 \tau_{\alpha j}^0 \sum_{\chi=1}^{M} \frac{(-\eta_\alpha)^{\chi-1}}{\chi!}\left(\boldsymbol{\tau}_\alpha^0.\nabla\right)^{\chi-1} p_\alpha \tag{6}$$

The superscript (*M*) in Eq. (6) refers to the generalized macrostresses which incorporate scale effects. This macrostress in Eq. (6) is the same as stresses in virial theorem [50] with this difference that in virial stresses, there is no gradient of microstresses and it doesn't explicitly contain scale parameter. It should be added that if the scale parameter in Eqs. (3) and (6) is set to zero, the CCM theory is obtained, as we expected.

The three-dimensional equations of motion in DM in the Cartesian coordinate system are given by [32]

$$\frac{\partial \sigma_{ij}^{(M)}}{\partial x_i} + f_i^* = \rho^* \frac{\partial^2 u_j}{\partial t^2} \tag{7}$$

where x_i ,$i = 1,2,3$ are the spatial Cartesian coordinates, u_j ,$j = 1,2,3$ are the displacement components, t is the time, and ρ^* and f^* are the three dimensional body force and mass density, respectively.

Now, the form of matrix $[\boldsymbol{A}]$ in Eq. (4) containing elastic macroconstants for a two-dimensional plane problem is obtained. For this purpose, Fig. 3 is considered wherein the $x_1 - x_2$ plane, three doublets are shown with equal angles between them.

The solution for the scale-less approximation in DM can be calculated directly from the associated continuum mechanical problem for an isotropic material.

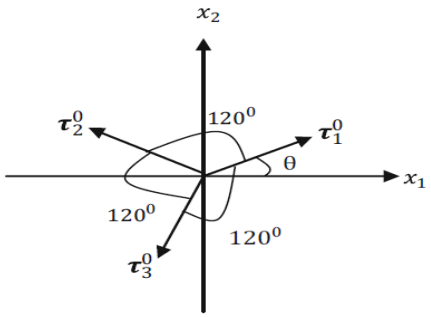

Fig.3
Three doublets with equal angle 120^0 between them.

For a two-dimensional problem in DM, the matrix $[\boldsymbol{A}]$ is a symmetric matrix of order three with the most general form [44]

$$[\boldsymbol{A}] = \begin{bmatrix} a & b & b \\ b & a & b \\ b & b & a \end{bmatrix} \tag{8}$$

It can be shown in [28] that the coefficients of tensor $[\boldsymbol{A}]$ are independent of direction thereby rendering the material isotropic. Furthermore, the coefficients a and b in matrix $[\boldsymbol{A}]$ under plane stress conditions are determined to be [1]

$$a = \frac{4}{9}\mu \frac{7\lambda + 10\mu}{\lambda + 2\mu} \,, b = \frac{4}{9}\mu \frac{\lambda - 2\mu}{\lambda + 2\mu} \tag{9}$$

One could use $b = 0$ as a quantitative guide to the applicability of a simpler constitutive relations such as Eq. (5). If $\lambda = 2\mu$ (or $\nu = \frac{1}{3}$) under plane stress conditions, from Eq. (9), it is concluded that $b = 0$ and

$$a = A_0 = \frac{8\mu}{3} = \frac{8G}{3} = E \tag{10}$$

3 DM MODEL OF CAR VIBRATION

Specific applications of DM have been developed for two-dimensional problems with regular particle packing microstructures. In particular, the two-dimensional hexagonal packing microstructure without internal atoms establishes three doublet axes at 120^0 angles as shown in Fig. 3.

In the remainder of this section, the governing equations for RBM vibration of SWCNTs are derived. Now, consider a SWCNT of length L, mean radius R, Young's modulus E, Poisson's ratio v and mass density ρ as shown in Fig. 4.

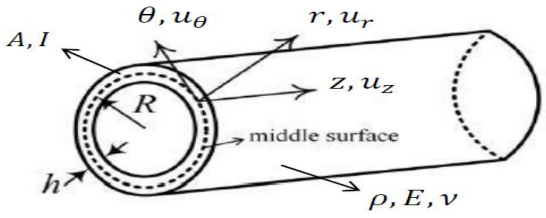

Fig.4
A nanotube in cylindrical coordinate.

In the cylindrical coordinates, the equations of motion are given by the following equations [1, 32]

$$\frac{\partial N_{zz}}{\partial z}+\frac{1}{r}\frac{\partial N_{\theta z}}{\partial \theta}+\rho f_z=\rho\frac{\partial^2 u_z}{\partial t^2} \tag{11}$$

$$\frac{\partial N_{z\theta}}{\partial z}+\frac{1}{r}\frac{\partial N_{\theta\theta}}{\partial \theta}+\frac{N_{\theta r}}{r}+\rho f_\theta=\rho\frac{\partial^2 u_\theta}{\partial t^2} \tag{12}$$

$$\frac{\partial N_{zr}}{\partial z}+\frac{1}{r}\frac{\partial N_{\theta r}}{\partial \theta}-\frac{N_{\theta\theta}}{r}+\rho f_r=\rho\frac{\partial^2 u_r}{\partial t^2} \tag{13}$$

$$\frac{\partial M_{zz}}{\partial z}+\frac{1}{r}\frac{\partial M_{\theta z}}{\partial \theta}+\rho\bar{l}_z=N_{zr} \tag{14}$$

$$\frac{\partial M_{z\theta}}{\partial z}+\frac{1}{r}\frac{\partial M_{\theta\theta}}{\partial \theta}+\frac{1}{r}M_{\theta r}+\rho\bar{l}_\theta=N_{\theta r} \tag{15}$$

$$\frac{M_{zr}}{\partial z}+\frac{1}{r}\frac{M_{\theta r}}{\partial \theta}-\frac{M_{\theta\theta}}{r}+\rho\bar{l}_r=N_{rr} \tag{16}$$

which are the equations of motion of a thin shell in the cylindrical coordinates.

Also, assuming that the shell-like body is thin, Eqs. (17) and (18) may be used to write the physical components N_{ij} and M_{ij} as:

$$N_{ij}=\int_{-\frac{h}{2}}^{\frac{h}{2}}\sigma_{ij}^{(M)}dz \quad ,i,j=1,2,3 \tag{17}$$

$$M_{ij}=\int_{-\frac{h}{2}}^{\frac{h}{2}}z\,\sigma_{ij}^{(M)}dz \quad ,i,j=1,2,3 \tag{18}$$

From Eq. (3), the microstrains with only three terms in the expansion can be written in cylindrical coordinates as:

$$\epsilon_\alpha = \boldsymbol{\tau}^0_\alpha.\left(\boldsymbol{\tau}^0_\alpha.\nabla\boldsymbol{u}\right)+\frac{1}{2}\eta_\alpha\left[\boldsymbol{\tau}^0_\alpha.\left(\boldsymbol{\tau}^0_\alpha.\nabla\right)\left(\boldsymbol{\tau}^0_\alpha.\nabla\boldsymbol{u}\right)\right]+\frac{1}{6}\eta_\alpha^2\left[\boldsymbol{\tau}^0_\alpha.\left(\boldsymbol{\tau}^0_\alpha.\nabla\right)\left(\boldsymbol{\tau}^0_\alpha.\nabla\right)\left(\boldsymbol{\tau}^0_\alpha.\nabla\boldsymbol{u}\right)\right] \tag{19}$$

where the gradient operator ∇ in cylindrical coordinates is given by

$$\nabla = \frac{\partial}{\partial r}\boldsymbol{e}_r+\frac{1}{r}\frac{\partial}{\partial\theta}\boldsymbol{e}_\theta+\frac{\partial}{\partial z}\boldsymbol{e}_z \tag{20}$$

Similarly, from Eq. (6), the macro- to microstress relations, to within three terms in the expansion, in the cylindrical coordinates may be written as:

$$\boldsymbol{\sigma}^{(M)} = \sum_{\alpha=1}^{n}\boldsymbol{\tau}^0_\alpha\boldsymbol{\tau}^0_\alpha\left\{\left(p_\alpha-\frac{1}{2}\eta_\alpha\boldsymbol{\tau}^0_\alpha.\left(\nabla p_\alpha\right)+\frac{1}{6}\eta_\alpha^2\left[\left(\boldsymbol{\tau}^0_\alpha.\nabla\right)\left(\boldsymbol{\tau}^0_\alpha.\nabla p_\alpha\right)\right]\right)\right\} \tag{21}$$

In this study, the following assumptions, known as Love's first approximation, for cylindrical shells are made [44]:

1. All points that lie on a normal to the middle surface before deformation do the same after the deformation. Then the transverse shear stresses $\sigma_{rz}^{(M)}$ and $\sigma_{\theta z}^{(M)}$ are assumed to be negligible.
2. Displacements are small compared to the shell thickness.
3. The normal stresses in the thickness direction ($\sigma_{rr}^{(M)}$) are negligible (planar state of stress).

As mentioned before, in the radial vibration, all carbon atoms move coherently in the radial direction creating a breathing-like vibration of the entire tube and in the axial vibration, the nanotube vibrates in the axial direction. The CAR is the mixing of two vibrations. If the nanotube is approximated by a homogeneous cylinder, the frequency of the radial vibration is linear with the inverse tube diameter [18]. Thus, with assumptions of axisymmetric and homogeneity for the entire tube in the RBM vibration, this implies that $\frac{\partial}{\partial\theta}=0,\frac{\partial}{\partial\mathrm{r}}=0$ and $u_\theta=0$. Considering such assumptions and neglecting body forces, Eqs. (32)- (37) reduce to

$$\frac{\partial N_{zz}}{\partial z}+\rho f_z=\rho\frac{\partial^2 u_z}{\partial t^2} \tag{22}$$

$$\frac{\partial N_{zr}}{\partial z}-\frac{N_{\theta\theta}}{r}+\rho f_r=\rho\frac{\partial^2 u_r}{\partial t^2} \tag{23}$$

As a result of the above assumptions, the gradient operator and the displacement vector are given by:

$$\nabla=\frac{\partial}{\partial z}\boldsymbol{e}_z\ ,\boldsymbol{u}=u_r\left(z\right)\boldsymbol{e}_r+u_z\left(z\right)\boldsymbol{e}_z \tag{24}$$

It is further assumed that all doublets originating from a common node have the same magnitudes, i.e., $\eta_a=\eta,a=1,2,3$.

As mentioned above, a SWCNT is constructed from three doublets having equal lengths and angles between them, an example of which is a Zigzag SWCNT ($\theta=0$ in Fig. 3) shown in Fig. 5.

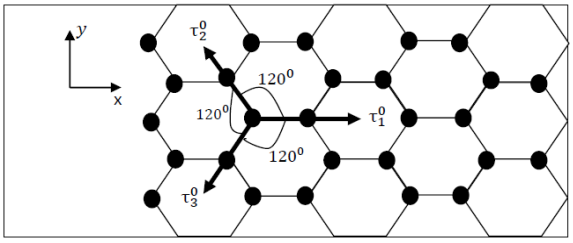

Fig.5
A Zigzag nanotube.

Considering Fig. 5, the director vectors in cylindrical coordinates can be expressed as:

$$\tau_{1r}^0 = 0\ ,\tau_{2r}^0 = 0\ ,\tau_{3r}^0 = 0 \tag{25}$$

$$\tau_{1\theta}^0 = 0\ ,\tau_{2\theta}^0 = cos\,30\ ,\tau_{3\theta}^0 = -cos\,30 \tag{26}$$

$$\tau_{1z}^0 = -1\ ,\tau_{2z}^0 = -cos\,60\ ,\tau_{3z}^0 = -cos\,60 \tag{27}$$

where z is in the axial direction and r and θ are in the radial and circumferential directions of the nanotube, respectively.

Substituting Eq. (24) into Eq. (19) and performing some algebraic manipulations detailed in Appendix A, it is found that

$$\begin{aligned} \epsilon_\alpha = {} & \frac{1}{r}\left(\tau_{\alpha\theta}^0\right)^2 u_r + \left(\tau_{\alpha z}^0\right)^2 \frac{\partial u_z}{\partial z} + \frac{1}{2}\eta_\alpha \left[\frac{2}{r}\tau_{\alpha z}^0 \left(\tau_{\alpha\theta}^0\right)^2 \frac{\partial u_r}{\partial z} + \left(\tau_{\alpha z}^0\right)^3 \frac{\partial^2 u_z}{\partial z^2}\right] + \\ & \frac{1}{6}\eta_\alpha^2 \left[-\frac{1}{r^3}\left(\tau_{\alpha\theta}^0\right)^4 u_r + \frac{3}{r}\left(\tau_{\alpha z}^0\right)^2 \left(\tau_{\alpha\theta}^0\right)^2 \frac{\partial^2 u_r}{\partial z^2} + \left(\tau_{\alpha z}^0\right)^4 \frac{\partial^3 u_z}{\partial z^3}\right] \end{aligned} \tag{28}$$

Inserting Eq. (28) into Eq. (4), the following equation for the microstresses is obtained

$$\begin{aligned} p_\alpha = A_0 \Bigg\{ & \frac{1}{r}\frac{1}{1-\nu^2}\left(\tau_{\alpha\theta}^0\right)^2 u_r + \left(\tau_{\alpha z}^0\right)^2 \frac{\partial u_z}{\partial z} + \frac{1}{2}\eta_\alpha \left[\frac{2}{r}\frac{1}{1-\nu^2}\tau_{\alpha z}^0 \left(\tau_{\alpha\theta}^0\right)^2 \frac{\partial u_r}{\partial z} + \left(\tau_{\alpha z}^0\right)^3 \frac{\partial^2 u_z}{\partial z^2}\right] + \\ & \frac{1}{6}\eta_\alpha^2 \left[-\frac{1}{r^3}\frac{1}{1-\nu^2}\left(\tau_{\alpha\theta}^0\right)^4 u_r + \frac{3}{r}\frac{1}{1-\nu^2}\left(\tau_{\alpha z}^0\right)^2 \left(\tau_{\alpha\theta}^0\right)^2 \frac{\partial^2 u_r}{\partial z^2} + \left(\tau_{\alpha z}^0\right)^4 \frac{\partial^3 u_z}{\partial z^3}\right] \Bigg\} \end{aligned} \tag{29}$$

Similarly, substituting p_α from Eq. (29) into Eq. (6) and taking note of Eq. (24), it is found that

$$\begin{aligned} \sigma_{ij}^{(M)} = A_0 \sum_{\alpha=1}^{3} \tau_{\alpha i}^0 \tau_{\alpha j}^0 \Bigg\{ & \frac{1}{r}\frac{1}{1-\nu^2}\left(\tau_{\alpha\theta}^0\right)^2 u_r + \left(\tau_{\alpha z}^0\right)^2 \frac{\partial u_z}{\partial z} + \frac{1}{12}\eta_\alpha^2 \\ & \left[-\frac{1}{r^3}\frac{1}{1-\nu^2}\left(\tau_{\alpha\theta}^0\right)^4 u_r + \frac{3}{r}\frac{1}{1-\nu^2}\left(\tau_{\alpha z}^0\right)^2 \left(\tau_{\alpha\theta}^0\right)^2 \frac{\partial^2 u_r}{\partial z^2} + \left(\tau_{\alpha z}^0\right)^4 \frac{\partial^3 u_z}{\partial z^3}\right] \Bigg\} \end{aligned} \tag{30}$$

This equation is the relation between the macrostresses and the displacements. Setting i and j equal to θ in Eq. (30), the following equation for the normal stress $\sigma_{zz}^{(M)}$ and $\sigma_{\theta\theta}^{(M)}$ are found to be

$$\begin{aligned} \sigma_{zz}^{(M)} = A_0 \sum_{\alpha=1}^{3} \Bigg\{ & \frac{1}{r}\frac{1}{1-\nu^2}\left(\tau_{\alpha z}^0\right)^2 \left(\tau_{\alpha\theta}^0\right)^2 u_r + \left(\tau_{\alpha z}^0\right)^4 \frac{\partial u_z}{\partial z} + \frac{1}{12}\eta_\alpha^2 \\ & \left[-\frac{1}{r^3}\frac{1}{1-\nu^2}\left(\tau_{\alpha z}^0\right)^2 \left(\tau_{\alpha\theta}^0\right)^4 u_r + \frac{3}{r}\frac{1}{1-\nu^2}\left(\tau_{\alpha z}^0\right)^4 \left(\tau_{\alpha\theta}^0\right)^2 \frac{\partial^2 u_r}{\partial z^2} + \left(\tau_{\alpha z}^0\right)^6 \frac{\partial^3 u_z}{\partial z^3}\right] \Bigg\} \end{aligned} \tag{31}$$

$$\sigma_{\theta\theta}^{(M)} = A_0 \sum_{\alpha=1}^{3} \left\{ \frac{1}{r} \frac{1}{1-\nu^2} \left(\tau_{\alpha\theta}^0\right)^4 u_r + \left(\tau_{\alpha\theta}^0\right)^2 \left(\tau_{\alpha z}^0\right)^2 \frac{\partial u_z}{\partial z} + \frac{1}{12}\eta_\alpha^2 \right.$$
$$\left. \left[-\frac{1}{r^3} \frac{1}{1-\nu^2} \left(\tau_{\alpha\theta}^0\right)^6 u_r + \frac{3}{r} \frac{1}{1-\nu^2} \left(\tau_{\alpha z}^0\right)^2 \left(\tau_{\alpha\theta}^0\right)^4 \frac{\partial^2 u_r}{\partial z^2} + \left(\tau_{\alpha\theta}^0\right)^2 \left(\tau_{\alpha z}^0\right)^4 \frac{\partial^3 u_z}{\partial z^3} \right] \right\} \tag{32}$$

If Eq. (31) and Eq. (32) are substituted into Eq. (17) and then integrated along the tube thickness, the following equations are obtained

$$N_{zz}^{(M)} =$$
$$A_0 A \sum_{\alpha=1}^{3} \left\{ \frac{1}{r} \frac{1}{1-\nu^2} \left(\tau_{\alpha z}^0\right)^2 \left(\tau_{\alpha\theta}^0\right)^2 u_r + \left(\tau_{\alpha z}^0\right)^4 \frac{\partial u_z}{\partial z} + \frac{1}{12}\eta_\alpha^2 \right.$$
$$\left. \left[-\frac{1}{r^3} \frac{1}{1-\nu^2} \left(\tau_{\alpha z}^0\right)^2 \left(\tau_{\alpha\theta}^0\right)^4 u_r + \frac{3}{r} \frac{1}{1-\nu^2} \left(\tau_{\alpha z}^0\right)^4 \left(\tau_{\alpha\theta}^0\right)^2 \frac{\partial^2 u_r}{\partial z^2} + \left(\tau_{\alpha z}^0\right)^6 \frac{\partial^3 u_z}{\partial z^3} \right] \right\} \tag{33}$$

$$N_{\theta\theta}^{(M)} =$$
$$A_0 h \sum_{\alpha=1}^{3} \left\{ \frac{1}{r} \frac{1}{1-\nu^2} \left(\tau_{\alpha\theta}^0\right)^4 u_r + \left(\tau_{\alpha\theta}^0\right)^2 \left(\tau_{\alpha z}^0\right)^2 \frac{\partial u_z}{\partial z} + \frac{1}{12}\eta_\alpha^2 \right.$$
$$\left. \left[-\frac{1}{r^3} \frac{1}{1-\nu^2} \left(\tau_{\alpha\theta}^0\right)^6 u_r + \frac{3}{r} \frac{1}{1-\nu^2} \left(\tau_{\alpha z}^0\right)^2 \left(\tau_{\alpha\theta}^0\right)^4 \frac{\partial^2 u_r}{\partial z^2} + \left(\tau_{\alpha\theta}^0\right)^2 \left(\tau_{\alpha z}^0\right)^4 \frac{\partial^3 u_z}{\partial z^3} \right] \right\} \tag{34}$$

Inserting Eq. (32) into Eq. (33) and Eq. (32) into Eq. (34), the two following coupled equations are obtained

$$A_0 \sum_{\alpha=1}^{3} \left\{ \frac{1}{r} \frac{1}{1-\nu^2} \left(\tau_{\alpha z}^0\right)^2 \left(\tau_{\alpha\theta}^0\right)^2 \frac{\partial u_r}{\partial z} + \left(\tau_{\alpha z}^0\right)^4 \frac{\partial^2 u_z}{\partial z^2} + \frac{1}{12}\eta_\alpha^2 \right.$$
$$\left. \left[-\frac{1}{r^3} \frac{1}{1-\nu^2} \left(\tau_{\alpha z}^0\right)^2 \left(\tau_{\alpha\theta}^0\right)^4 \frac{\partial u_r}{\partial z} + \frac{3}{r} \frac{1}{1-\nu^2} \left(\tau_{\alpha z}^0\right)^4 \left(\tau_{\alpha\theta}^0\right)^2 \frac{\partial^3 u_r}{\partial z^3} + \left(\tau_{\alpha z}^0\right)^6 \frac{\partial^4 u_z}{\partial z^4} \right] \right\} = \rho \frac{\partial^2 u_z}{\partial t^2} \tag{35}$$

$$A_0 \sum_{\alpha=1}^{3} \left\{ -\frac{1}{r} \frac{1}{1-\nu^2} \left(\tau_{\alpha\theta}^0\right)^4 u_r - \left(\tau_{\alpha\theta}^0\right)^2 \left(\tau_{\alpha z}^0\right)^2 \frac{\partial u_z}{\partial z} - \frac{1}{12}\eta_\alpha^2 \right.$$
$$\left. \left[-\frac{1}{r^3} \frac{1}{1-\nu^2} \left(\tau_{\alpha\theta}^0\right)^6 u_r + \frac{3}{r} \frac{1}{1-\nu^2} \left(\tau_{\alpha z}^0\right)^2 \left(\tau_{\alpha\theta}^0\right)^4 \frac{\partial^2 u_r}{\partial z^2} + \left(\tau_{\alpha\theta}^0\right)^2 \left(\tau_{\alpha z}^0\right)^4 \frac{\partial^3 u_z}{\partial z^3} \right] \right\} = \rho r^2 \frac{\partial^2 u_r}{\partial t^2} \tag{36}$$

To find the frequency of CAR of the nanotube, one solution for the CAR vibration of the nanotube are assumed to be of the form

$$u_z(z,t) = U_z \cos\left(\frac{n\pi}{L} z\right) e^{i\omega^{(\eta)} t} \tag{37}$$

$$u_r(z,t) = U_r \sin\left(\frac{n\pi}{L} z\right) e^{i\omega^{(\eta)} t} \tag{38}$$

where W and $\omega^{(\eta)}$ are the amplitude and frequency of the CAR vibration, respectively. Superscript η in $\omega^{(\eta)}$ indicates the natural frequency with scale effects. Substituting Eqs. (35) and (36) into Eqs. (33) and (34) yields

$$A_0\sum_{\alpha=1}^{3}\left\{\frac{1}{r}\frac{1}{1-\nu^2}\left(\tau_{\alpha z}^0\right)^2\left(\tau_{\alpha\theta}^0\right)^2\left(\frac{n\pi}{L}\right)U_r-\left(\tau_{\alpha z}^0\right)^4\left(\frac{n\pi}{L}\right)^2U_z+\frac{1}{12}\eta_\alpha^2\right.$$
$$\left.\left[-\frac{1}{r^3}\frac{1}{1-\nu^2}\left(\tau_{\alpha z}^0\right)^2\left(\tau_{\alpha\theta}^0\right)^4\left(\frac{n\pi}{L}\right)U_r-\frac{3}{r}\frac{1}{1-\nu^2}\left(\tau_{\alpha z}^0\right)^4\left(\tau_{\alpha\theta}^0\right)^2\left(\frac{n\pi}{L}\right)^3U_r+\left(\tau_{\alpha z}^0\right)^6\left(\frac{n\pi}{L}\right)^4U_z\right]\right\}=-\rho\omega^2U_z \tag{39}$$

$$A_0\sum_{\alpha=1}^{3}\left\{-\frac{1}{r}\frac{1}{1-\nu^2}\left(\tau_{\alpha\theta}^0\right)^4U_r-\left(\tau_{\alpha\theta}^0\right)^2\left(\tau_{\alpha z}^0\right)^2\left(\frac{n\pi}{L}\right)U_z-\frac{1}{12}\eta_\alpha^2\right.$$
$$\left.\left[-\frac{1}{r^3}\frac{1}{1-\nu^2}\left(\tau_{\alpha\theta}^0\right)^6U_r-\frac{3}{r}\frac{1}{1-\nu^2}\left(\tau_{\alpha z}^0\right)^2\left(\tau_{\alpha\theta}^0\right)^4\left(\frac{n\pi}{L}\right)^2U_r-\left(\tau_{\alpha\theta}^0\right)^2\left(\tau_{\alpha z}^0\right)^4\left(\frac{n\pi}{L}\right)^3U_z\right]\right\}=-\rho r\omega^2U_r \tag{40}$$

Eqs. (37) and (38) can be written in the following matrix form

$$\begin{bmatrix}\frac{1}{1-\nu^2}\left[\frac{1}{r}\left(\tau_{\alpha z}^0\right)^2\left(\tau_{\alpha\theta}^0\right)^2\left(\frac{n\pi}{L}\right)-\frac{1}{12}\eta_\alpha^2\frac{1}{r^3}\left(\tau_{\alpha z}^0\right)^2\left(\tau_{\alpha\theta}^0\right)^4\left(\frac{n\pi}{L}\right)-\frac{1}{12}\eta_\alpha^2\frac{3}{r}\left(\tau_{\alpha z}^0\right)^4\left(\tau_{\alpha\theta}^0\right)^2\left(\frac{n\pi}{L}\right)^3\right] & \\ \frac{1}{1-\nu^2}\left[-\frac{1}{r}\left(\tau_{\alpha\theta}^0\right)^4+\frac{1}{12}\eta_\alpha^2\frac{1}{r^3}\left(\tau_{\alpha\theta}^0\right)^6+\frac{1}{12}\eta_\alpha^2\frac{3}{r}\left(\tau_{\alpha z}^0\right)^2\left(\tau_{\alpha\theta}^0\right)^4\left(\frac{n\pi}{L}\right)^2\right]+\frac{\rho r}{E}\omega^2 & \\ -\left(\tau_{\alpha z}^0\right)^4\left(\frac{n\pi}{L}\right)^2+\frac{1}{12}\eta_\alpha^2\left(\tau_{\alpha z}^0\right)^6\left(\frac{n\pi}{L}\right)^4+\frac{\rho}{E}\omega^2 & \\ -\left(\tau_{\alpha\theta}^0\right)^2\left(\tau_{\alpha z}^0\right)^2\left(\frac{n\pi}{L}\right)+\frac{1}{12}\eta_\alpha^2\left(\tau_{\alpha\theta}^0\right)^2\left(\tau_{\alpha z}^0\right)^4\left(\frac{n\pi}{L}\right)^3 & \end{bmatrix}\begin{bmatrix}U_r\\U_z\end{bmatrix}=0 \tag{41}$$

To have a unique nonzero solution for the above equations, the determinant of the coefficients must be zero. Then, solving the determinant equations, yields the following two frequencies

$$\left(\omega_1^{(\eta)}\right)^2=\frac{E^2}{2\rho^2r}\left(-b+\sqrt{d}\right) \tag{42}$$

$$\left(\omega_2^{(\eta)}\right)^2=\frac{E^2}{2\rho^2r}\left(-b-\sqrt{d}\right) \tag{43}$$

wherein $\omega_1^{(\eta)}$ and $\omega_2^{(\eta)}$ are defined as higher band and lower band frequencies, respectively. *b* and *d* are defined by the following equations

$$b=\frac{\rho}{E}\frac{1}{1-\nu^2}\left[-\frac{1}{r}\left(\tau_{\alpha\theta}^0\right)^4+\frac{1}{12}\eta_\alpha^2\frac{1}{r^3}\left(\tau_{\alpha\theta}^0\right)^6+\frac{1}{12}\eta_\alpha^2\frac{3}{r}\left(\tau_{\alpha z}^0\right)^2\left(\tau_{\alpha\theta}^0\right)^4\left(\frac{n\pi}{L}\right)^2\right]+$$
$$\frac{\rho r}{E}\left[-\left(\tau_{\alpha z}^0\right)^4\left(\frac{n\pi}{L}\right)^2+\frac{1}{12}\eta_\alpha^2\left(\tau_{\alpha z}^0\right)^6\left(\frac{n\pi}{L}\right)^4\right] \tag{44}$$

$$d=b^2-4\frac{\rho^2r}{E^2}\frac{1}{1-\nu^2}\left\{\left[-\left(\tau_{\alpha z}^0\right)^4\left(\frac{n\pi}{L}\right)^2+\frac{1}{12}\eta_\alpha^2\left(\tau_{\alpha z}^0\right)^6\left(\frac{n\pi}{L}\right)^4\right]\right.$$
$$\left[-\frac{1}{r}\left(\tau_{\alpha\theta}^0\right)^4+\frac{1}{12}\eta_\alpha^2\frac{1}{r^3}\left(\tau_{\alpha\theta}^0\right)^6+\frac{1}{12}\eta_\alpha^2\frac{3}{r}\left(\tau_{\alpha z}^0\right)^2\left(\tau_{\alpha\theta}^0\right)^4\left(\frac{n\pi}{L}\right)^2\right]$$
$$+\left[-\frac{1}{r}\left(\tau_{\alpha z}^0\right)^2\left(\tau_{\alpha\theta}^0\right)^2\left(\frac{n\pi}{L}\right)+\frac{1}{12}\eta_\alpha^2\frac{1}{r^3}\left(\tau_{\alpha z}^0\right)^2\left(\tau_{\alpha\theta}^0\right)^4\left(\frac{n\pi}{L}\right)+\frac{1}{12}\eta_\alpha^2\frac{3}{r}\left(\tau_{\alpha z}^0\right)^4\left(\tau_{\alpha\theta}^0\right)^2\left(\frac{n\pi}{L}\right)^3\right]$$
$$\left.\left[-\left(\tau_{\alpha\theta}^0\right)^2\left(\tau_{\alpha z}^0\right)^2\left(\frac{n\pi}{L}\right)+\frac{1}{12}\eta_\alpha^2\left(\tau_{\alpha\theta}^0\right)^2\left(\tau_{\alpha z}^0\right)^4\left(\frac{n\pi}{L}\right)^3\right]\right\} \tag{45}$$

In Eqs. (40) and (41), $\omega_1^{(\eta)}$ and $\omega_2^{(\eta)}$ are the lower and higher band frequencies, respectively. Finally, upon substituting the components of the director vectors from Eqs. (42) and (43) into Eq. (35) and taking note of Eq. (8), the natural frequencies for the coupled axial-radial direction for a Zigzag SWCNTs are obtained. The advantage of these simple expressions is that they show the dependency of the CAR frequencies on the mechanical and geometrical properties of the SWCNT.

In Eq. (39), if $U_r = 0$, then following equation for the natural frequency is obtained for Zigzag SWCNT:

$$\left(\omega^{(\eta)}\right)^2 = \frac{E}{\rho}\left(1-\frac{1}{12}\eta^2\right) \tag{46}$$

which is in complete agreement with the natural frequency for the Zigzag SWCNTs in axial vibration obtained in [21].

Similarly, in Eq. (40), if $U_z = 0$, the following equation for the natural frequency is obtained for Zigzag SWCNT in RBM vibration:

$$\left(\omega^{(\eta)}\right)^2 = \frac{1}{r^2}\frac{E}{\rho\left(1-\nu^2\right)}\left(1-\frac{11}{72}\frac{\eta^2}{r^2}\right) \tag{47}$$

which is in complete agreement with the RBM frequency for the Zigzag SWCNTs obtained in [44].

From Eqs. (42) -(47), it is obvious that major differences exist between DM and CCM models but with increase in the length and/or the radius of the tube, the difference between the natural frequency of axial and radial vibration with and without the scale parameter decreases and the two frequencies converge to the same value. It is also observed that the presence of the scale parameter η decreases the natural frequency in comparison with the CCM frequency.

In DM, basic equations of scaling microdynamics for local interactions with homogeneous medium can be written as follow [1]

$$\rho\ddot{u}_i = \sum_{\kappa=2,4,\ldots}^{R=2M} C_{ijk_1k_2\ldots k_\kappa}\frac{\partial^\kappa u_i}{\partial x_{k_1}\partial x_{k_2}\ldots\partial x_{k_\kappa}} = C_{ijkl}u_{j,kl} + C_{ijklrs}u_{j,klrs} + C_{ijklrspq}u_{j,klrspq} + \ldots \tag{48}$$

where

$$C_{ijk_1k_2\ldots k_\kappa} = 2A_0\sum_{\alpha=1}^{n}\tau_{\alpha i}^0\tau_{\alpha j}^0\tau_{\alpha k_1}^0\tau_{\alpha k_2}^0\ldots\tau_{\alpha k_\kappa}^0\frac{\eta_\alpha^{\kappa-2}}{\kappa!} \tag{49}$$

For CAR vibration mode of SWCNTs studied in this paper, Eq. (48) is reduced to Eqs. (39) and Eq. (40), respectively. It is noted that the nonscale macromodulus C_{ijkl}, corresponding to $k=2$, is indeed independent of θ, i.e., isotropic in the plane. On the contrary, the macromoduli $C_{ijk_1k_2\ldots k_\kappa}$ for $k=4,6,\ldots$ are anisotropic. Then, it may be concluded that in the first approximation, $k=2$, Eq. (48) model the continuum-like behavior of solids, whereas in the other approximations, $k=4,6,\ldots$ Eq. (48) also reflect discrete-like features of the solid, in a manner that increases with *k* [1]. Therefore, it can be concluded that DM is capable of modeling solids in view of their dual and to some extent contradictory discrete continuous nature. The power of such dual-representation capability is evident in the discussion of isotropy. The basal plane of the doublets arrangement (Fig. 3) is isotropic only in the continuum (nonscale) approximation. Thus, isotropy is a scale-related notion. In fact, no material may be argued to be isotropic at all dimensional scales, down to its most elementary component level [1].

4 RRSULTS AND DISCUSSION

In this section, comparison between the results obtained herein using DM and the available theoretical results are presented. Experimentally, the CAR natural frequencies are related to angular frequency ω via $f = \frac{w}{2\pi C}$ where, $C = 2.99 \times 10^{10} \frac{cm}{s}$ is the velocity of light in the vacuum. This relation is used in Tables 1 and 2 below to report the frequencies in cm^{-1}. In Table 1 and 2, the material properties of SWCNT are taken to be: Young's modulus $E = 1TPa$, mass density $\rho = 2300 \frac{kg}{m^3}$ and Poisson's ratio $\nu = 0.2$ [44]. In the DM model, the scale parameter used is the carbon-carbon bond length $\eta = 0.1421nm$ [28]. For calculating the lower band CAR natural frequency, the material properties of SWCNT are taken to be: Young's modulus $E = 0.938 - 0:999\ TPa$, mass density $\rho = 2491 \frac{kg}{m^3}$ and Poisson's ratio $\nu = 0.147 - 0.251$ [21].

Tables 1 and 2 show the CAR frequencies of different Zigzag and Armchair SWCNTs based on the available analytical and experimental results presented here. The first column shows the *n* and *m* chiral indices of the nanotube; the second and third columns show the SWCNT diameter (*d*, in *nm*) and length (*L*, *nm*), respectively. The next two columns are the analytical results.

From Tables 1 and 2, it can be seen that the doublet mechanical predictions of the CAR frequencies of different SWCNTs are in good agreement with the available results. Variation of the lower band and higher band frequency are proportional to axial vibration and RBM vibration, respectively. Only a shift is expected depending on the interactions between the two modes. The difference between lower band with axial vibration frequency and also higher band with RBM frequency may be due to the interactions and coupling effect between axial and radial vibration. The coupling effect increases the higher band frequency in comparison with RBM frequency while decreases the lower band frequency in comparison with the axial vibration frequency.

These tables also show that at large diameters, the higher band CAR frequency of the SWCNTs are almost equivalent with the RBM frequencies of the corresponding SWCNTs. Unlike the lower band CAR frequency, the difference between the lower band CAR frequency and the axial vibration frequency of the tube are nearly constant with increasing the tube diameters.

Table 1

Comparison between higher band frequencies of CAR (cm^{-1}) with axial frequency (cm^{-1}) for different SWCNTs.

Tube (*n, m*)	Radius (*nm*)	Length (*nm*)	Lower band frequency	Axial frequency obtained in [28] using DM	Axial frequency obtained in [47] using MM
(5,0)	0.1869	5.5425	20.5738	58.2742	58.006
(5,5)	0.3222	9.7043	12.1202	34.1490	33.730
(10,0)	0.3716	11.2969	10.4338	29.5432	29.633
(8,8)	0.5146	15.5261	7.4983	21.1931	21.161
(9,9)	0.5787	17.3879	6.6924	18.9240	18.902
(16,0)	0.5939	18.1303	6.2999	17.8380	18.329
(10,10)	0.6429	19.2503	6.1224	17.0932	17.077
(11,11)	0.7071	21.1130	5.5113	15.5933	15.574
(20,0)	0.7422	22.2966	5.2188	14.7792	14.691
(13,13)	0.8355	25.0718	4.6400	13.1312	13.120
(23,0)	0.8534	25.5246	4.5567	12.9049	12.837
(15,15)	0.9640	29.2642	3.9770	11.2558	11.244
(26,0)	0.9646	29.5587	3.9357	11.1437	11.092

Table 2

Comparison between higher band frequencies of CAR (cm^{-1}) with RBM (cm^{-1}) for different SWCNTs.

Tube (*n, m*)	Diameter (*nm*)	Length (*nm*)	Higher band frequency	RBM frequency obtained in [31] using DM	Axial frequency obtained in [34] using experimental result
(3,3)	0.4069	6.0	582.3223	534.2	549.3
(6,0)	0.4698	7.0	507.9977	469.8	475.7
(4,4)	0.5425	8.0	440.4292	407.7	412.0
(7,0)	0.5481	9.0	436.4168	405.3	407.8
(8,0)	0.6264	10.0	382.7157	356.0	356.8
(5,5)	0.6781	10.5	353.5446	328.7	329.6
(9,0)	0.7047	11.0	340.7216	317.4	317.2
(10,0)	0.7830	12.0	306.9981	286.2	285.4
(6,6)	0.8138	12.5	295.2212	275.1	274.6
(11,0)	0.8613	13.0	279.3290	260.5	259.5
(12,0)	0.9397	14.0	256.1957	239.1	237.8
(7,7)	0.9494	14.5	253.3823	236.4	235.4
(8,8)	1.0850	15.0	222.1132	207.2	206.0
(13,0)	1.0180	15.5	236.5436	220.9	219.5
(14,0)	1.0963	16.0	219.8109	205.2	203.9
(15,0)	1.1746	17.0	205.2309	191.7	190.3
(9,9)	1.2206	17.5	197.4705	184.3	183.1
(16,0)	1.2529	18.0	192.4621	179.8	178.4
(17,0)	1.3312	19.0	181.1872	169.3	167.9
(10,10)	1.3563	19.5	177.7780	166.0	164.8
(18,0)	1.4095	20.0	171.1587	159.9	158.6
(19,0)	1.4878	21.0	162.1811	151.5	150.2
(20,0)	1.5661	22.0	154.0975	144.0	142.7

The calculations for frequencies in CAR vibration are given in graphical form in Figs. 6-8. In Fig. 6, variation of the CAR frequencies for SWCNTs (higher band and lower band) with respect to the tube diameter are plotted. According to this figure, increase in the diameter of the nanotube results in decrease in the higher band frequencies for all tubes. This decreasing is more apparent for lower radii. Since scale effect is more apparent for smaller wave lengths, beyond a certain tube radius, frequencies approach to a certain value. Lower band CAR frequency is approximately independent to tube diameter as axial frequency are independent to tube diameter. The results agree with reported experimental results obtained under different conditions [28, 31].

Variations of the CAR frequencies for SWCNTs (higher band and lower band) with respect to the tube length are plotted in Fig. 7. According to this figure, increase in the length of the nanotube results in decrease in the two higher band and lower band frequencies for all tubes. This decreasing is more apparent for lower lengths. Since scale effect is more apparent for smaller wave lengths, beyond a certain tube length, frequencies approach to a certain value. The results also agree with reported experimental results obtained under different conditions [28, 31].

In Fig. 8, variation of the CAR frequencies with scale parameter for (13, 0) Zigzag and (13, 13) Armchair nanotubes is shown for different mode number. It can be seen that higher band CAR frequency will decrease if the scale parameter increases. This decreasing is more apparent for higher scale parameter. However, lower band CAR frequency does not change appreciably with scale parameter. It can also be concluded that increasing mode vibration of the nanotube results in increase in the CAR frequencies for both types of nanotubes.

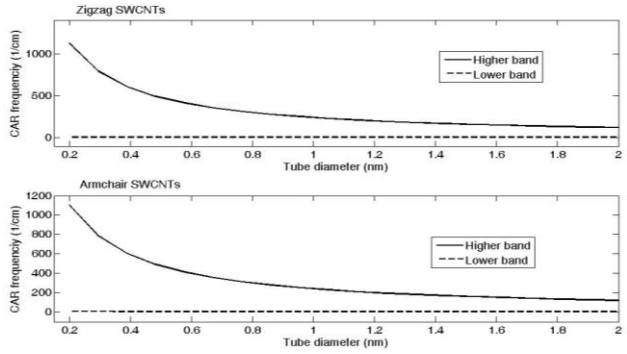

Fig.6
Variation of the CAR frequencies with tube diameter for Zigzag and Armchair nanotubes.

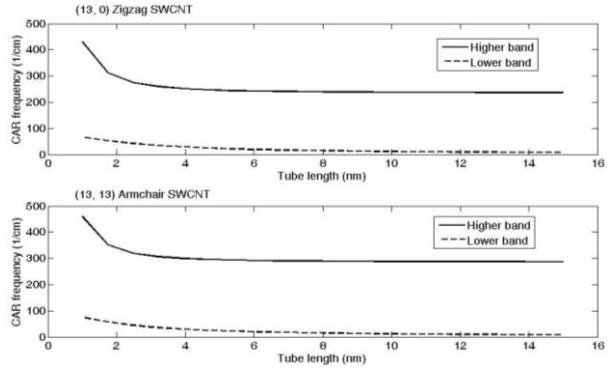

Fig.7
Variation of CAR frequencies with tube length for Zigzag and Armchair SWCNTs.

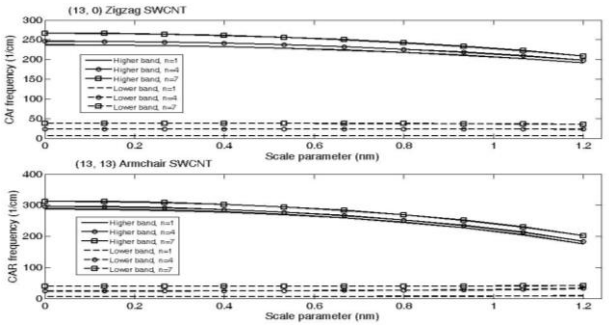

Fig.8
Variation of CAR frequencies with scale parameter for different mode number for (13, 0) Zigzag and (13, 13) Armchair SWCNTs.

5 CONCLUSIONS

In this paper, a detailed investigation of the CAR frequency of the SWCNT based on DM has been presented. The equation of motion for CAR vibration of the SWCNT based on DM is derived. It is the first time that DM has been used to analyze the CAR vibration of SWCNTs. To obtain the CAR frequency equation, the equation of motion is solved. The following points are particularly noted. Firstly, the CAR vibration frequencies of the SWCNT depend on the geometric (radius and scale parameter) and mechanical properties (Young's modulus, density and Poisson's ratio) of the nanotube. Secondly, the scale effects decrease higher band CAR frequencies or the nanotube's stiffness is lessened in comparison with the predictions of the CCM theory. However, lower band CAR frequencies will not change considerably with scale effect. Also, the effect of the scale parameter is more pronounced for the nanotubes with smaller length and radii. Thirdly, higher band CAR frequencies decrease with increasing in tube radius and length while lower band CAR frequency are constant with changing tube radius. It is notable that for a nanotube with sufficiently large radius and length, the scale effect becomes insignificant and the governing equation can be reduced to the classical equation and DM and CCM frequencies converge to a single value. To show the accuracy and ability of this method, the CAR frequencies obtained herein compared with the frequencies of RBM and axial vibration mode in available literature. It was shown that the higher band and lower band CAR frequency are in agreement with RBM and axial vibration frequencies, respectively.

REFERENCES

[1] Fatahi-Vajari A., Imam A., 2016, Torsional vibration of single-walled carbon nanotubes using doublet mechanics, *Zeitschrift für angewandte Mathematik und Physik* **67**:81.
[2] Banks H. T., Hu S., Kenz Z. R., 2011, A brief review of elasticity and viscoelasticity for solids, *Advances in Applied Mathematics and Mechanics* **3**(1): 1-51.
[3] Granik V.T., Ferrari M., 1993, Microstructural mechanics of granular media, *Mechanics of Materials* **15**: 301-322.
[4] Eringen A.C., 1972, Nonlocal polar elastic continua, *International Journal of Engineering Science* **10**: l-16.
[5] Yang Y., Lim C.W., 2012, Non-classical stiffness strengthening size effects for free vibration of a nonlocal nanostructure, *International Journal of Mechanical Sciences* **54**: 57-68.
[6] Mindlin R.D., Eshel N.N., 1968, On first strain-gradient theories in linear elasticity, *International Journal of Solids and Structures* **4**: 109-124.

[7] Dell'Isola F., Della Corte A., Giorgio I., 2017, Higher-gradient continua: The legacy of Piola, Mindlin, Sedov and Toupin and some future research perspectives, *Mathematics and Mechanics of Solids* **22**(4): 852-872.
[8] Polizzotto C., 2014, Stress gradient versus strain gradient constitutive models within elasticity, *International Journal of Solids and Structures* **51**: 1809-1818.
[9] Ramasubramaniam A., Carter E.A., 2007, Coupled quantum–atomistic and quantum–continuum mechanics methods, *Materials Research* **32**: 913-918.
[10] Dove M.T., 2007, An introduction to atomistic simulation methods, *Seminarios de la SEM* **4**: 7-37.
[11] Carcaterra A., 2015, Quantum euler beam—QUEB: modeling nanobeams vibration, *Continuum Mechanics and Thermodynamics* **27**: 145-156.
[12] Friak M., Hickel T. Grabowski B., Lymperakis L., Udyansky A., Dick A., Ma D., Roters F., Zhu L.F., Schlieter A., Kuhn U., Ebrahimi Z., Lebensohn R.A., Holec D., Eckert J., Emmerich H., Raabe D., Neugebauer J., 2011, Methodological challenges in combining quantum-mechanical and continuum approaches for materials science applications, *The European Physical Journal Plus* **126**(101): 1-22.
[13] Khodabakhshi P., Reddy J. N., 2016, A unified beam theory with strain gradient effect and the von Karman nonlinearity, *ZAMM* **97**: 70-91.
[14] Beheshti A., 2017, Generalization of strain-gradient theory to finite elastic deformation for isotropic materials, *Continuum Mechanics and Thermodynamics* **29**: 493-507.
[15] Kiani K., 2014, Axial buckling analysis of vertically aligned ensembles of single-walled carbon nanotubes using nonlocal discrete and continuous models, *Acta Meccanica* **225**: 3569-3589.
[16] Fatahi-Vajari A. , Azimzadeh Z., 2018, Analysis of nonlinear axial vibration of single-walled carbon nanotubes using Homotopy perturbation method, *Indian Journal of Physics* **92**: 1425-1438.
[17] Kiani K., 2014, In- and out-of-plane dynamic flexural behaviors of two-dimensional ensembles of vertically aligned single-walled carbon nanotubes, *Physica B, Condensed Matter* **449**: 164-180.
[18] Aydogdu M., 2012, Axial vibration analysis of nanorods (carbon nanotubes) embedded in an elastic medium using nonlocal elasticity, *Mechanics Research Communications* **43**: 34-40.
[19] Kiani K., 2018, Application of nonlocal higher-order beam theory to transverse wave analysis of magnetically affected forests of single-walled carbon nanotubes, *International Journal of Mechanical Sciences* **138-139**: 1-16.
[20] Ferrari M., Granik V.T., Imam A., Nadeau J., 1997, *Advances in Doublet Mechanics*, Springer-Verlag, Berlin.
[21] Fatahi-Vajari A., Imam A., 2016, Axial vibration of single-walled carbon nanotubes using doublet mechanics, *Indian Journal of Physics* **90**(4): 447-455.
[22] Granik V.T., 1978, *Microstructural Mechanics of Granular Media*, Institute of Mechanics of Moscow State University, Russian.
[23] Kojic M., Vlastelica I., Decuzzi P., Granik V.T., Ferrari M., 2011, A finite element formulation for the doublet mechanics modeling of microstructural materials, *Computer Methods in Applied Mechanical Engineering* **200**: 1446-1454.
[24] Xin J., Zhou L.X., Ru W.J., 2009, Ultrasound attenuation in biological tissue predicted by the modified doublet mechanics model, *Chinese Physics Letters* **26**(7): 074301.1-074301.4.
[25] Gentile F., Sakamoto J., Righetti R., Decuzzi P., Ferrari M., 2011, A doublet mechanics model for the ultrasound characterization of malignant tissues, *Journal of Biomedical Science and Engineering* **4**: 362-374.
[26] Fang J.Y., Jue Z., Jing F., Ferrari M., 2004, Dispersion analysis of wave propagation in cubic-tetrahedral assembly by doublet mechanics, *Chinese Physics Letters* **21**(8): 1562-1565.
[27] Sadd M.H., Dai Q., 2005, A comparison of micro-mechanical modeling of asphalt materials using finite elements and doublet mechanics, *Mechanics of Materials* **37**: 641-662.
[28] Fatahi-Vajari A., Imam A., 2016, Lateral vibrations of single-layered graphene sheets using doublet mechanics, *Journal of Solid Mechanics* **8**(4): 875-894.
[29] Lin S.S., Shen Y.C., 2005, Stress fields of a half-plane caused by moving loads-resolved using doublet mechanics, *Soil Dynamics and Earthquake Engineering* **25**: 893-904.
[30] Sadd M.H., 2005, *Elasticity Theory, Applications, and Numeric*, Elsevier Butterworth-Heinemann, Burlington.
[31] Lee A.P., Lee J., Ferrari M., 2006, *BioMEMS and Biomedical Nanotechnology, Biological and Biomedical Nanotechnology*, Springer, New York.
[32] Fatahi-Vajari A., 2018, A new method for evaluating the natural frequency in radial breathing like mode vibration of double-walled carbon nanotubes, *ZAMM* **98**(2): 255-269.
[33] Maultzsch J., Telg H., Reich S., Thomsen C., 2005, Radial breathing mode of single-walled carbon nanotubes: Optical transition energies and chiral-index assignment, *Physical Review B* **72**: 205438.1-205438.16.
[34] Basirjafari S., EsmaielzadehKhadem S., Malekfar R., 2013,Validation of shell theory for modeling the radial breathing mode of a single-walled carbon nanotube, *International Journal of Engineering: Transactions A* **26**(4): 447-454.
[35] Szabó A., Perri C., Csató A., Giordano G., Vuono D., Nagy J.B., 2010, Synthesis methods of carbon nanotubes and related materials, *Materials* **3**: 3092-3140.
[36] Prasek J., Drbohlavova J., Chomoucka J., Hubalek J., Jasek O., Adamc V., Kizek R., 2011, Methods for carbon nanotubes synthesis, *Journal of Materials Chemistry* **21**: 15872-15884.
[37] Hongjie D., 2002, Carbon nanotubes: synthesis, integration, and properties, *American Chemical Society* **35**: 1035-1044.

[38] Zhang Y. Y., Wang C. M., Tan V. B. C., 2009, Assessment of timoshenko beam models for vibrational behavior of single-walled carbon nanotubes using molecular dynamics, *Advances in Applied Mathematics and Mechanics* **1**(1): 89-106.

[39] Kiani K., 2018, Nonlocal free dynamic analysis of periodic arrays of single-walled carbon nanotubes in the presence of longitudinal thermal and magnetic fields, *Computers and Mathematics with Applications* **75**: 3849-3872.

[40] Ghorbanpour Arani A., Mosallaie Barzoki A. A., Kolahchi R., Loghman A., 2011, Pasternak foundation effect on the axial and torsional waves propagation in embedded DWCNTs using nonlocal elasticity cylindrical shell theory, *Journal of Mechanical Science and Technology* **25**(9): 2385-2391.

[41] Basirjafari S., EsmaeilzadehKhadem S., Malekfar R., 2013, Radial breathing mode frequencies of carbon nanotubes for determination of their diameters, *Current Applied Physics* **13**: 599-609.

[42] Kiani K., 2014, Nonlocal discrete and continuous modeling of free vibration of stocky ensembles of vertically aligned single-walled carbon nanotubes, *Current Applied Physics* **14**(8): 1116-1139.

[43] Das S.L., Mandal T., Gupta S.S., 2013, Inextensional vibration of zig-zag single-walled carbon nanotubes using nonlocal elasticity theories, *International Journal of Solids and Structures* **50**: 2792-2797.

[44] Fatahi-Vajari A., Imam A., 2016, Analysis of radial breathing mode vibration of single-walled carbon nanotubes via doublet mechanics, *ZAMM* **96**(9): 1020-1032.

[45] Li C.F., Zhou S.H., Liu J., Wen B.C., 2014, Coupled lateral-torsional-axial vibrations of a helical gear-rotor-bearing system, *Acta Mechanica Sinica* **30**(5): 746-761.

[46] Kiani K., 2014, Nanoparticle delivery via stocky single-walled carbon nanotubes: A nonlinear-nonlocal continuum-based scrutiny, *Composite Structures* **116**: 254-272.

[47] Gupta S.S., Batra R.C., 2008, Continuum structures equivalent in normal mode vibrations to single-walled carbon nanotubes, *Computational Materials Science* **43**: 715-723.

[48] Lin S.Y., 1995, Coupled vibration and natural frequency analysis of isotropic cylinders or disks of finite dimensions, *Journal of Sound and Vibration* **185**(2): 193-199.

[49] Ren F., Wang B., Chen S., Yao Z., Bai B., 2016, Nonlinear model and qualitative analysis for coupled axial/torsional vibrations of drill string, *Shock and Vibration* **2016**: 1646814.

[50] Subramaniyan A.K., Sun C.T., 2008, Continuum interpretation of virial stress in molecular simulations, *International Journal of Solids and Structures* **45**: 4340-4346.